

EULER'S ELASTICA AND CURVATURE BASED INPAINTINGS

TONY F. CHAN, SUNG HA KANG AND JIANHONG SHEN *

Abstract. Image inpainting is a special image restoration problem for which image prior models play a crucial role. Euler's elastica was first introduced by Mumford [21] to computer vision as a prior curve model. By functionalizing the elastica energy, Masnou and Morel [19] proposed an elastica based variational inpainting model. The current paper is intended to contribute to the development of its mathematical foundation, and the study of its properties and connections to the earlier works of Bertalmio, Sapiro, Caselles, and Ballester [2] and Chan and Shen [6, 7]. A computational scheme based on numerical PDEs is presented, which allows the handling of topologically complex inpainting domains.

Key words. Inpainting, elastica, prior models, Bayesian method, variational method, bounded variation, curvature, Euler-Lagrange equations, transportation, diffusion, numerical method.

AMS subject classifications. Primary: 94A08; Secondary: 68U10, 65K10.

1. Introduction. Among museum conservators and restoration artists, inpainting refers to the practice of retouching or recovering damaged ancient paintings [9, 30]. The goal is to remove the cracks or recover the missing patches in an undetectable manner.

The term of *digital inpainting* was initially introduced into image processing by Bertalmio, Sapiro, Caselles, and Ballester [2]. The authors were the first to apply the PDE method to inpaintings, by introducing their innovative construction of a third-order PDE. Equally important in [2] is that the authors demonstrated the broad applications of digital inpaintings in film restorations, text removal, scratch removal, and special effects in movies. The same group of authors have also lately developed a variational inpainting model based on a joint cost functional on the gradient vector field and grey values [1]. An earlier variational inpainting model was studied by Masnou and Morel [19] in the context of disocclusion in computer vision (also see the coming sections). Recently, Chan and Shen proposed the *total variation* (TV) inpainting model [7] and a new PDE inpainting model based on *curvature driven diffusions* (CDD) [6]. In [7], Chan and Shen also introduced interesting new applications in digital zooming and edge-based image coding schemes.

Inpainting is essentially an interpolation problem. What makes image interpolation highly non-trivial is the complexity of image functions as discussed in more details in [7]. A simple but often sufficient mathematical model for (non-texture) images is the BV (*bounded variation*) space, where one of the most crucial low-level visual features—edge, is legalized (see Rudin, Osher and Fatemi [27, 28], and Chambolle and Lions [4], for examples). Yet, in both the approximation community and that of numerical analysis, as far as we know, there has been very little work on interpolations in BV spaces. It is partially because that such problems have rarely emerged in the literature outside image analysis, and perhaps more importantly, that the problem itself is not well-posed. The latter is much easier to see from a simple 1-D example. Imagine we know the values (or even the derivatives) of a function f at $a - h$ and $a + h$. If f is smooth, then as $h \rightarrow 0$, we can apply smooth interpolants

* Chan and Kang are with Department of Mathematics, UCLA, Los Angeles, CA 90095, ({chan, skang}@math.ucla.edu); Shen is with School of Mathematics, University of Minnesota, Minneapolis, MN 55455, (shen@math.umn.edu). Research is supported by grants from NSF under grant number DMS-9973341 and from ONR under N00014-96-1-0277.

such as Lagrange’s and Hermit’s to infer the values of f on $(a - h, a + h)$ with certain guaranteed degree of precision. But for a BV function f , all such smooth interpolants fail to work properly no matter how small h is, since a “widthless” jump can always occur in $(a - h, a + h)$. This is the specialty of BV functions: by the TV (total variation) Radon measure, a single point is allowed to have nonzero mass, which makes the corresponding interpolation problem ill-posed generally.

The good news is that images as BV functions are not too intractable. Each image is a 2-D projection of a window of our 3-D world, in which individual objects often have their geometric or surface reflection regularities. Such regularities weaken the ill-posedness of the inpainting problem.

Given an image, if we partially cover it up with a piece of paper of moderate size, and ask a person to guess what is behind in the original image, almost surely, everyone will come up with a “rational” best guess. For example, if a green apple was partially occluded by the paper cover, then one tends to estimate the incomplete boundary first, followed by an inpainting with the green color inside. All these decisions are realized by best guesses, or more scientifically, by the Bayesian inference [10, 14, 22]. The two ingredients of Bayesian inference are the *prior* model and *data* model. The data model is simple for inpainting problems: the available data is simply a part of a complete image that we try to restore. Thus the prior model plays a crucial role in our inferring process or decision making. For the thought experiment mentioned above, the *a priori* knowledge of the shape and color of an apple is helpful for a person to make a meaningful inpainting.

In order to develop an inpainting model that applies to general problems, on one hand, one should never rely on the *prior* model of a specific class of image objects (such as apples), and on the other hand, the model must integrate into it the above-mentioned regularities of image objects to better condition the ill-posedness. The Rudin-Osher-Fatemi’s TV (total variation) [28] and Mumford-Shah’s smoothest-object-and-shortest-edge models [23] are two well-known general prior models that have been widely applied in image restorations and segmentations. As Chan and Shen pointed out in [6, 7], for the inpainting problem, they are less suitable in some large-scale situations when they fail to realize the so-called *Connectivity Principle* and create visible corners due to their straight line connections.

In the current paper, we study a variational inpainting model that is based on a prior model for plane curves — Euler’s elastica. The gap between a prior model for curves and that for images is bridged by the level sets (or isophotes): generally, a curve prior model can always be “lifted” to an image prior model by being imposed on all the isophotes of an image (similar to the *co-area* formula in the theory of BV functions [12]). Indeed, this is how Masnou and Morel first proposed this model for image inpaintings in [19]. Our current paper is intended to study the mathematical foundation and properties of inpainting models based on elasticas and curvatures, the connections to the existing works on PDE or variational inpaintings, and construct schemes that are based on numerical PDEs, instead of Masnou and Morel’s linear programming algorithm [19]. From the computational point of view, numerical PDE is a more flexible approach for inpaintings in that it frees one from laboring on edge detection or pixel coupling along the boundaries, and also that it puts no topological restriction on inpainting domains [19].

Euler’s elastica was first seriously introduced and studied in computer vision by Mumford [21] as a prior curve model. They were employed in disocclusion programs as an edge model to smoothly connect occluded edges and T-junctions [24], thus used

as *nonlinear splines* as first discussed by Birkhoff and De Boor [3] in approximation theory.

The paper starts with a brief introduction to Euler's elastica, and Mumford's Bayesian rationale for it being a curve model (Section 2). Then as in classical approximation theory, in Section 3, we first study the generic (non-texture) local image models in order to study inpainting as an interpolation problem. By the method of moving frames, we are able to inpaint or interpolate the missing T-junctions or corners inside the inpainting domain based on the elastica interpolants. We then explain the approach that leads to Masnou and Morel's algorithm on individually "engineering" isophotes [19]. A level-set [26] kind of idea then formally "lifts" this isophote based model to a variational functional that acts directly on gray level images. The rest of the paper is devoted to the mathematical analysis and understanding of this elastica based variational inpainting model.

In Section 4, by introducing the concept of *weak curvature* of a general BV function, we legitimize the functionalization of the elastica energy in BV spaces. The direct (variational) method for the elastica inpainting is generally difficult due to the lack of classical fine properties (such as convexity and semi-continuities). But for the extreme case of TV inpaintings, we are able to establish rigorously the existence theorems based on the theory of functions with bounded variations. We also discuss why the non-uniqueness of the solutions to a general inpainting model should be somehow appreciated instead of being cursed. In this main section, we also prove that the curvature power p in Masnou and Morel's p -elastica model must stay below 3 in order to allow the existence of a generic stationary pixel, namely a pixel x_0 , where $\nabla u(x_0) = 0$, yet the Hessian matrix $H_u(x_0)$ is non-degenerate. The last part of the section discusses various relaxation schemes for the companion constraints of the inpainting energy.

In Section 5, we derive the formal Euler-Lagrange equation for a general curvature-based inpainting model. The most interesting and important result is on the behavior of the flux field of the energy. It turns out that the flux field and its associated divergence form perfectly unify the earlier work of Bertalmio et al. [2] on transportation based inpaintings and that of Chan and Shen on CDD (curvature driven diffusion) based inpaintings [6]. We conjecture that transportation and diffusion are the two universal infinitesimal mechanisms for any low-level inpainting schemes.

Numerical schemes and computational examples consist into the last section.

we wish that the current paper can inspire much more works from our community in the near future.

2. Euler's Elastica and its Bayesian Rationale. A curve Γ is said to be *Euler's elastica* if it is the equilibrium curve of the elasticity energy:

$$E_2[\gamma] = \int_{\gamma} (a + b\kappa^2) ds, \quad (2.1)$$

where ds denotes the arc length element, $\kappa(s)$ the scalar curvature, and a, b two positive constant weights. Extra constraints may include the positions and normal directions of the two ends. Euler in 1744 obtained the energy in studying the steady shape of a thin and torsion-free rod under external forces [16].

Since both the arc length and curvature are intrinsic geometric features of a curve, the elastica energy naturally extends to the curves living on a general Riemannian manifold M . For example, if M is embedded in a Euclidean space R^N , then a curve

γ on M can be expressed by the embedded coordinates:

$$s \rightarrow \vec{x}(s) = (x_1(s), \dots, x_N(s)).$$

Then $\vec{t} = d\vec{x}/ds$ is the tangent, and $\Pi_{\vec{x}}d\vec{t}/ds = \kappa\vec{n}$ defines the curvature, with $\Pi_{\vec{x}}$ representing the orthogonal projection from $T_{\vec{x}}R^N$ to $T_{\vec{x}}M$. For a general Riemannian manifold M , the intrinsic derivative $d\vec{t}/ds$ is defined by the Levi-Civita connection or covariant derivative (see Chern et al. [8] for example). The attention to the extension of elasticas onto a general manifold is motivated by inpainting problems on arbitrary surfaces in R^3 , for example, to inpaint an incomplete image on the surface of a Coke can in computer graphics.

By calculus of variations, it can be shown from the energy formula (2.1) that an elastica must satisfy

$$2\kappa''(s) + \kappa^3(s) = \frac{a}{b}\kappa(s).$$

For example, Mumford gives a detailed derivation in [21]. More generally, if the elastica lives on a Riemannian surface, then there will be an extra term due to the curving of the surface:

$$2\kappa''(s) + \kappa^3(s) + 2G(s)\kappa(s) = \frac{a}{b}\kappa(s),$$

with $G(s)$ denoting the Gaussian curvature of the surface. More studies in elasticas on general Riemannian manifolds can be found in Langer and Singer [15].

Elastica was first seriously studied from the computer vision point of view in Mumford's paper [21], whose introduction section provides a delightful view on the mathematical history of Euler's elastica. According to [21], the key link between elastica and computer vision is founded on the interpolation capability of elasticas, as initially proposed by Birkhoff and De Boor [3]. Such "nonlinear splines" [3], like classical polynomial splines, are useful tools to complete the broken or occluded edges of objects in the 2-D projection of a 3-D scene [24].

A remarkable feature of elasticas revealed by Mumford [21] is their Bayesian rationale, which positively supports the role of elasticas in image and vision analysis as an interpolation tool. It also sheds light on the choice of "2" for the curvature power in the energy formula (2.1). Here we present a slightly polished version of Mumford's argument. This Bayesian rationale also supports the idea of applying elasticas to the inpainting problem.

Consider the random walk of a drunk initially staying at the origin of a 2-D ground. Assume that each step is straight. For some given fixed integer N , we try to understand the distribution of all possible N -step polygonal walks. The moving characteristics are

- (a) Let h_k denote the step size of the k -th step. Then $\{h_k : k = 1, 2, \dots, N\}$ are i.i.d of exponential type $\lambda \exp(-\lambda h)$ for some positive mean $1/\lambda$.
- (b) Let θ_k denote the orientation of the k -th step, measured by the angle between the walking direction and the x -axis, and define $\theta_0 = 0$. Let $\Delta\theta_k = \theta_k - \theta_{k-1}$ ($k = 1, 2, \dots, N$) denote the turn made at the k -th step. The basic assumption is that, at each step k , the larger the step size h_k is, the more uncertain the turn $\Delta\theta_k$ will become. Precisely, $\Delta\theta_k$ is a Gaussian of $N(0, h_k\sigma)$ for some commonly shared deviation σ . Yet

$$\{n_k = \Delta\theta_k/h_k : k = 1, 2, \dots, N\}$$

is an independent set and also independent of all the h_k 's.

Thus, an N -step polygonal walk γ is completely determined by the data

$$\{h_1, \dots, h_N\} \cup \{\Delta\theta_1, \dots, \Delta\theta_N\},$$

and the likelihood is quantified by

$$\begin{aligned} & \lambda^N \exp(-\lambda(h_1 + \dots + h_N)) dh_1 \cdots dh_N \\ & \times (\sqrt{2\pi}\sigma)^{-N} \exp\left(-\frac{1}{2\sigma^2}[(\Delta\theta_1/h_1)^2 + \dots + (\Delta\theta_N/h_N)^2]\right) dn_1 \cdots dn_N. \end{aligned}$$

Thus, up to a multiplicative constant, the probability density function is exactly

$$\exp\left(-\lambda L(\gamma) - \frac{1}{2\sigma^2} \|\kappa^2\|_\gamma\right),$$

where L denotes the length and $\|\kappa^2\|_\gamma$ the discrete analogy of $\int_\gamma \kappa^2 ds$. Therefore, the minimization of the elastica energy (2.1) with $a = \lambda$ and $b = 1/(2\sigma^2)$ is equivalent to the Maximum Likelihood (ML) estimation of such random curves. This is the Bayesian world view hidden in elasticas, which also rationalizes the elastica idea for image inpaintings.

REMARK 1. Notice that the drunk walking model presented above does not come from the discrete sampling of Brownian motions, since for the latter (in 2-D), h^2 (not h) is exponential and the turn $\Delta\theta$ is uniform along the unit circle. The dependence of the turns on the step sizes makes the paths smoother than the sampling of Brownian motions, which makes the model a valuable curve model in computer vision, where regularity is important. Figure 2.1 shows a computer simulation of the paths.

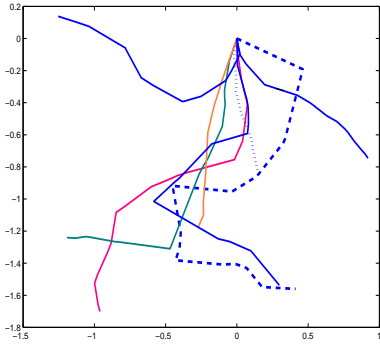


FIG. 2.1. Some sample paths for the drunk's walking.

3. Local (Non-texture) Image Models and Elastica Isophotes.

3.1. Generic local (non-texture) image models. To model inpaintings (of non-texture images), it is important to first start with local and small inpainting domains. Focusing on locality is a common practice in numerical mathematics, where from differentiation, integration, interpolation, to optimization, most well-known numerical schemes (such as the Runge-Kutta schemes, Simpson's integration rule, and the Newton-Raphson searching strategy for zeros or valleys) are all inspired by the local models of the target functions, such as the linear model, parabolic model, and so on [13, 29]. Digital inpainting, after all, is the numerical interpolation of 2-D images. Therefore, it is crucial to first understand what an image looks like locally.

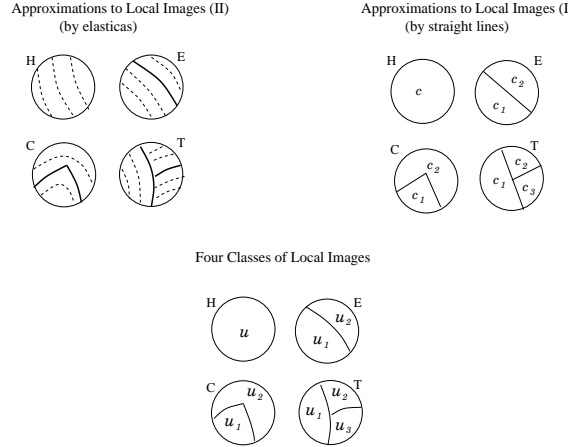


FIG. 3.1. *Local (non-texture) image models and their approximations*

Imagine that we have a small aperture, say, a round plain lens with a small radius r , and we only focus on the part that is captured within when it is moved over a 2-D gray scale image. Suppose that the image contains mostly man-made (non-texture) objects, and their characteristic scale $l \gg r$. What kind of (local) image patches will be observed most frequently?

They can be grouped into four classes, labeled by “H,” “E,” “C,” and “T” (see Figure 3.1).

- (a) Class H. A local image patch belongs to this class if and only if it falls within the *homogeneous* region of an object. Such a patch has very little intensity variation.
- (b) Class E. This occurs when the aperture captures a fraction of the smooth *edge* between two objects or homogeneous regions.
- (c) Class C. Like class E, but the aperture captures a recognizable *corner*. Corners are also a universal feature of man-made objects, from tables, windows, books, to posters.
- (d) Class T. This is the case when the aperture captures a *T-junction*. T-junction is an important cue for occlusion and therefore the perceptual reconstruction of object orders in the lost dimension of range [24]. A local T-junction patch is characterized by three homogeneous gray scales u_1 , u_2 , and u_3 , and two smooth edges – one meets the boundary at its two ends while the other at one end only due to occlusion.

Notice that homogeneous regions are 2-D objects, edges are 1-D objects, and both corners and T-junctions are isolated 0-D objects. Therefore, heuristically, in terms of the probability (or frequency) of being observed through a small aperture, we have the following relation:

$$\text{Prob}(H) \gg \text{Prob}(E) \gg \text{Prob}(C) \text{ or } \text{Prob}(T).$$

Of course, the probabilities do not necessarily represent their perceptual importance in terms of vision inference. In fact, it seems that often the scattered singular features can generate strong response from the vision system and contain crucial perceptual information (such as depth).

Notice that class C is indeed very much “man-made” like its ancestors in our 3-D world, in the sense that a local engineering (or perturbation) of the corner can easily change a class C patch to a class E patch. In this sense class C is unstable.

3.2. Local edge interpolation by elasticas: moving frames. Suppose an image u_0 has a local patch D missing, and we try to inpaint $u_0|_D$ based on the available information surrounding D .

By checking the boundary (or nearby) data along D , we can easily determine which class $u_0|_D$ belongs to: class H, class E, or class T (without a priori knowledge, one can never tell apart class C from class E based on the boundary information only). The existence of a corner or the exact configuration of the T-shape inside the inpainting domain will need extra information or requires additional models and algorithms (especially for the coupling of the three end points in the T-junction case). For the moment, let us assume that eventually we do know the right class that $u_0|_D$ belongs to.

A first level of approximation for each class of patches will be based on the *straight line* curve model (refer to the upper right panel in Figure 3.1). For a class H type, we can average the available boundary pixel values and inpaint $u_0|_D$ by this mean value c . For a class E type, we connect the two edge ends on the boundary by a straight line and inpaint the two objects u_1 and u_2 by their boundary mean values c_1 and c_2 . For a class C type, we make two separate straight shoots from the two boundary end points into the inpainting domain. The orientations follow their cue left outside D . The two straight lines generate a corner and also segment the patch D into two objects u_1 and u_2 . Then u_1 and u_2 are inpainted by their boundary mean values. For the last class T, we connect the coupled two boundary end points by a straight line, and shoot from the third one straightly toward the inside of D , as for class C. Then the three segmented objects u_1, u_2 and u_3 are inpainted by their boundary mean values c_1, c_2 and c_3 .

A second level of approximation is based on the *elastica* curve model (the upper left panel in Figure 3.1). That is, we shall interpolate the boundary end points by elasticas, instead of straight line segments. We can also improve the inpainting accuracy by approximating the isophotes by elasticas in the resulting segmented objects, instead of the constant approximations. Therefore, we need first to inpaint the missing edges (smooth, corner, or T-junction) to reduce class E, C, T to class H.

Along the boundary, each end point can be represented by (p, \vec{n}) , with p denoting its position and \vec{n} the normal to the edge, which can be computed from the available image outside the inpainting domain D .

- (a) For class E, we employ the elastica Γ that satisfies the boundary conditions (p_1, \vec{n}_1) and (p_2, \vec{n}_2) to inpaint the missing smooth edge.
- (b) For class C, to inpaint the corner, we take a *moving frame* approach. The corner is represented by an affine frame $(p; \vec{n}'_1, \vec{n}'_2)$, with p denoting its unknown position, and \vec{n}'_1 and \vec{n}'_2 the two unknown unit normals to the smooth edges coming from the boundary end points (p_1, \vec{n}_1) and (p_2, \vec{n}_2) . For each i , the energy (2.1) of the elastica that meets the requirement at (p_i, \vec{n}_i) and (p, \vec{n}'_i) is denoted by

$$E_2((p_i, \vec{n}_i), (p, \vec{n}'_i)).$$

Then the corner is inpainted by a joint optimization:

$$\min_{(p; \vec{n}'_1, \vec{n}'_2)} E_2((p_1, \vec{n}_1), (p, \vec{n}'_1)) + E_2((p_2, \vec{n}_2), (p, \vec{n}'_2)). \quad (3.1)$$

For example, if in the elastica energy (2.1), we choose a large ratio b/a (or $a = 0$ for the extremal case), then the solution to (3.1) shall be very close to the straight line shooting method mentioned in the first level of approximation.

- (c) For class T, we first inpaint the two coupled end points by an elastica Γ , just as what has been done for class E. To inpaint the occluded edge from the clue of the third boundary end point (p_3, \vec{n}_3) , we take again the *the moving frame* approach. Let (p, \vec{n}'_3) denote the junction position and the normal direction of the occluded edge. Then, the junction inpainting is completed by solving

$$\min_{(p, \vec{n}'_3)} E_2((p_3, \vec{n}_3), (p, \vec{n}'_3)). \quad (3.2)$$

Here an admissible p must stay on the disoccluded edge Γ .

3.3. Local inpainting by individually engineering the isophotes. After the feature edges have all been interpolated, all the four classes of local image inpaintings are essentially reduced to the inpainting of class H, the homogeneous patches. Such patches can also be inpainted by having the broken isophotes interpolated by elasticas *one by one* from the boundary information. This is exactly the idea underlying Masnou and Morel's dynamical programming algorithm [19].

Generically, one can assume that the missing smooth patch $u_0|_D$ is *regular* in the sense that it lies close to a regular point where ∇u_0 is non-zero (or by first applying a small step of Gaussian diffusion). Thus the isophotes of u_0 on D are well defined and distinguishable, and each Γ_λ is uniquely labeled by its gray level $u_0 \equiv \lambda$.

The trace of each Γ_λ on the boundary tells the coupling rule of boundary pixels. Suppose $p_1, p_2 \in \partial\Omega$ share the same gray level λ , and the normals computed from the available image data outside D are \vec{n}_1 and \vec{n}_2 . Then we inpaint the λ -isophote Γ_λ by an elastica Γ'_λ :

$$\Gamma'_\lambda = \operatorname{argmin}_{\gamma_\lambda \vdash ((p_1, \vec{n}_1), (p_2, \vec{n}_2))} \int_{\gamma_\lambda} (a + b\kappa^2) ds = \operatorname{argmin}_{\gamma_\lambda \vdash ((p_1, \vec{n}_1), (p_2, \vec{n}_2))} E_2[\gamma_\lambda], \quad (3.3)$$

where \vdash means subjecting to the (boundary) conditions, i.e., γ_λ goes through p_1 and p_2 , and $\dot{\gamma}_\lambda \perp \vec{n}_i$ at the two ends.

As λ varies according to the available boundary data u_0 , (3.3) gives a family of (and theoretically infinitely many) elasticas. On the other hand, if we denote this bundle of elasticas by

$$\mathcal{F}' = \{\Gamma'_\lambda : 0 \leq \lambda \leq 1\},$$

then it is easy to see that \mathcal{F}' is also the minimizer of the following energy for all boundary admissible curve bundles $\mathcal{F} = \{\gamma_\lambda : 0 \leq \lambda \leq 1\}$:

$$E[\mathcal{F}] = \int_0^1 E_2[\gamma_\lambda] d\lambda, \quad (3.4)$$

or more generally,

$$E_w[\mathcal{F}] = \int_0^1 w(\lambda) E_2[\gamma_\lambda] d\lambda, \quad (3.5)$$

with some positive weight function $w(\lambda)$ (whose influence in applications will be explained later). Although the last two formulations seem to show hopes of engineering the elastica interpolations in a mass production manner, there still exist two potential problems due to the lack of communications among the elasticas:

- (1) Problem 1: two different elastica interpolants Γ'_λ and Γ'_μ with $\lambda \neq \mu$ can meet inside the inpainting domain D , while the original two isophotes never.
- (2) Problem 2: even putting on hold Problem 1, generally, it is not guaranteed that the elastica bundle

$$\mathcal{F}' = \{\Gamma'_\lambda : 0 \leq \lambda \leq 1\}$$

does “weave” the entire inpainting domain D and leaves no “holes.” Thus, the inpainting can still be incomplete.

These issues have been taken care in Masnou and Morel’s algorithm [19]. Another perhaps more convenient alternative approach is to work with the level-set function u_D instead. (The similar philosophy has now made the *level-set method* of Osher and Sethian [26] a great success in the numerical computations of various interface motion problems.) An admissible curve bundle $\mathcal{F} = \{\gamma_\lambda\}_\lambda$, which not only satisfies the boundary conditions, but also avoids the above mentioned two problems, is uniquely and fully characterized by an inpainting function u_D that is “tangent” to u_0 along ∂D . Conversely, working with u_D instead of the individual isophotes automatically avoids the above two problems. Thus, first we need to translate the elasticity energies (3.4) or (3.5) into ones that are directly applicable to the inpainting function u_D .

4. The Elastica Inpainting Model.

4.1. The functionalized elastica energy. Let $u = u_D$ be an admissible inpainting. Then along any isophote $\gamma_\lambda : u \equiv \lambda$, the curvature of the oriented curve is given by

$$\kappa = \nabla \cdot \vec{n} = \nabla \cdot \left(\frac{\nabla u}{|\nabla u|} \right),$$

as now well known and frequently applied in image analysis [20]. On the other hand, let dt denote the length element along the normal direction \vec{n} (or along the steepest ascent curve), then we have

$$\frac{d\lambda}{dt} = |\nabla u| \quad \text{or} \quad d\lambda = |\nabla u| dt.$$

Therefore, the integrated elastica energy (3.5) now passes on to u by

$$J[u] = E_w[\mathcal{F}] \tag{4.1}$$

$$= \int_0^1 w(\lambda) \int_{\gamma_\lambda:u=\lambda} (a + b\kappa^2) ds d\lambda \tag{4.2}$$

$$= \int_1^0 \int_{\gamma_\lambda:u=\lambda} w(u) \left(a + b \left(\nabla \cdot \frac{\nabla u}{|\nabla u|} \right)^2 \right) |\nabla u| dt ds \tag{4.3}$$

$$= \int_D w(u) \left(a + b \left(\nabla \cdot \frac{\nabla u}{|\nabla u|} \right)^2 \right) |\nabla u| dx, \tag{4.4}$$

since dt and ds represents a couple of orthogonal length elements. Now the energy is completely expressed in terms of the inpainting u itself. Notice that this formal derivation is much alike the co-area formula for BV functions [12].

The weight function $w(\lambda)$ can be set to 1. In applications, we can also define it by looking at the histogram $h(\lambda)$ of the given image. ($h(\lambda)$ denotes the frequency

of pixels with gray level λ .) The histogram of an image typically consists of several “humps,” each of which corresponds to an object. Since perceptually the regularity of the boundaries (or edges) defining the 2-D shapes of the objects is most sensitive to human observers, we may weigh high along such edges whose gray values typically lie near the “valleys” of the histogram. Therefore we may choose the weight function in the form of

$$w(\lambda) = W(1 - h(\lambda)),$$

with $W = W(h)$ being a suitable positive and increasing function.

The functionalized energy $J[u]$ together with suitable boundary conditions seem to formulate naturally an inpainting model. But we need to further clarify its meaning.

4.2. Admissible inpaintings and the weak form of curvature. From the moment on, let us consider the functionalized Euler’s elastica energy

$$J_2[u] = \int_D \left(a + b \left(\nabla \cdot \frac{\nabla u}{|\nabla u|} \right)^2 \right) |\nabla u| \, dx, \quad (4.5)$$

with the conditions that

$$u|_{\Omega \setminus D} = u_0|_{\Omega \setminus D}, \quad \int_{\partial D} |\nabla u| = 0, \quad \text{and } |\kappa(p)| < \infty \quad \text{a.e. along } \partial D, \quad (4.6)$$

where a.e. is in the sense of Hausdorff measure.

We have assumed that the original complete image u_0 (typically on a square domain Ω) belongs to $BV(\Omega)$ and has the property that

$$\int_{\partial D} |\nabla u_0| = 0, \quad (4.7)$$

in the sense of Radon measure $\int |\nabla u_0|$. Under such an assumption, the second boundary condition on u follows naturally. Another more explicit way is based on the *trace* of BV functions [12]. Let u^- and u^+ denote the interior and exterior traces of u along ∂D with respect to D . Then we have:

$$\int_{\partial D} |\nabla u| = \int_{\partial D} |u^+ - u^-| \, d\mathcal{H}_1.$$

Thus the second condition is equivalent to the continuity condition

$$u^- = u^+ = u_0^+, \quad \text{a.e. along } \partial D \text{ by } d\mathcal{H}_1.$$

We shall call assumption (4.7) on the original complete image *the feasibility condition* for all low-level inpaintings (i.e. inpaintings which do not depend on global feature recognitions or learning). It requires that there is no *essential* overlapping between the boundary of the inpainting domain D and the edges of 2-D objects in an image. Imagine the worst opposite situation. Suppose we have an image u_0 which pictures a lady’s face with clearly outlined red lips, and we now create the inpainting domain D by cutting the image just along the outer edges of the upper and lower lips. Then the boundary of D coincides with the edges of a 2-D object, and we have an entire object missing! Any inpainting scheme, without the help of more advanced knowledge (such as face recognition), will just paint the missing domain based on the

surrounding pixel values and create a human face without a mouth. A low-level inpainting, after all, is not expected to *create* a new object, but just to *complete* objects based on the hints they left outside the inpainting domain.

Finally, the last condition in (4.6) demands finite curvatures along the inpainting boundary. Therefore a sudden turn of isophotes is not permitted along ∂D , and the condition is thus a first order continuity constraint.

Despite that the quantity "curvature" for a BV function has been used for both the elastica energy and boundary condition, its meaning has very much stayed at a formal level, since an average BV function lacks the necessary regularity for discussing curvatures in the ordinary sense.

Therefore we introduce the concept of *weak curvature*, which may not be the only possibility of generalization, but seems to be general enough to serve image analysis.

Suppose $u \in \text{BV}(D)$. Then

$$d_u \nu = \int |\nabla u|$$

is a Radon measure on D . Recall that the TV norm is defined in the distributional sense:

$$\int_D |\nabla u| = \sup_{\mathbf{g} \in C_0^1(D, B_1)} \int_D u \cdot \nabla \cdot \mathbf{g} \, dx,$$

where B_1 denotes the unit ball centered at the origin in R^2 . Let $\text{supp}(d_u \nu)$ denote the support of the TV measure. Then for any $p \in \text{supp}(d_u \nu)$, on any of its small neighborhood N_p ,

$$d_u \nu(N_p) = \int_{N_p} |\nabla u| > 0.$$

Let ρ be a fixed radially symmetric non-negative mollifier with compact support and unit total integral, and set (for 2-D)

$$\rho_\sigma = \frac{1}{\sigma^2} \rho\left(\frac{x}{\sigma}\right) \quad \text{and} \quad u_\sigma = \rho_\sigma * u.$$

Then we define the *weak absolute curvature* $\tilde{\kappa}(p)$ of u at p by

$$\tilde{\kappa}(p) = \limsup_{\sigma \rightarrow 0} \left| \nabla \cdot \left(\frac{\nabla u_\sigma}{|\nabla u_\sigma|} \right)(p) \right|, \quad (4.8)$$

where for those σ 's which give $|\nabla u_\sigma(p)| = 0$, we define $\nabla \cdot (\nabla u_\sigma / |\nabla u_\sigma|)$ to be ∞ . Finally, for any pixel p outside $\text{supp}(d_u \nu)$, we assign 0 to $\tilde{\kappa}(p)$, since u is a.e. a constant near a neighborhood of p . Thus the weak absolute curvature is well-defined everywhere for an arbitrary BV function.

There are two important situations in image analysis in which the weak curvature is indeed the ordinary isophote or edge curvature for $p \in \text{supp}(d_u \nu)$:

PROPOSITION 4.1. *Suppose u is C^2 near p , and $\nabla u(p) \neq \mathbf{0}$. Then $\tilde{\kappa}(p) = |\kappa(p)|$.*

Proof. Assume that the mollifier is supported on the unit ball B_1 . From the definition of convolution

$$u_\sigma(q) = \rho_\sigma * u(q) = \int_{B_1} \rho(y) u(q + \sigma y) \, dy,$$

it is easy to see that there is a small neighborhood N_p and some positive number a , such that $u_\sigma(q)$ is C^2 over $(\sigma, q) \in (-a, a) \times N_p$. Since ∇u is continuous and non-vanishing at p , we can further refine N_p and a , so that all $\nabla u(q + \sigma y)$ (with $(\sigma, q, y) \in (-a, a) \times N_p \times B_1$) are concentrated enough around $\nabla u(p)$. Then thank to the averaging property of the mollifier, all $\nabla u_\sigma(q) = (\nabla u)_\sigma(q)$ are non-vanishing, which makes

$$\vec{n}_\sigma(q) = \nabla u_\sigma(q) / |\nabla u_\sigma(q)|$$

C^1 on $(-a, a) \times N_p$. Then

$$\kappa_\sigma(q) = \nabla \cdot \vec{n}_\sigma(q)$$

is well-defined on N_p and continuous in σ , especially, at p ,

$$|\kappa(p)| = \lim_{\sigma \rightarrow 0} |\kappa_\sigma(p)| = \tilde{\kappa}(p).$$

□

The second case is when p lies on an intensity edge between two objects.

PROPOSITION 4.2. *Suppose an oriented curve segment γ is a C^2 sub-manifold in D . Assume that near a given pixel $p \in \gamma$, to one side of γ , $u = c^+$, and to the other side, $u = c^-$, two constant gray values. Then $\tilde{\kappa}(p) = |\kappa(p)|$.*

Proof. Since curvature is a second order local feature, we can replace γ near p by the curvature circle with radius $r = 1/|\kappa(p)|$ and center $q = p - r\vec{n}$, where \vec{n} is one of the unit normal vectors at p . Then both the data (c^+, c^-) and the geometry γ are locally rotationally invariant (with respect to the center) in a neighborhood of p . So is u . Since the mollifier ρ is radially symmetric and compactly supported, as long as σ is small enough, $u_\sigma = \rho_\sigma * u$ must also be locally rotationally invariant with respect to the center, which means locally near p , γ is also an isophote of u_σ . Thus under the same orientation of γ ,

$$\kappa_\sigma(p) = \kappa(p),$$

especially, $\tilde{\kappa}(p) = \lim_\sigma |\kappa_\sigma(p)| = |\kappa(p)|$. This completes the proof. □

One useful property of $\tilde{\kappa}$ which can be proven easily is its invariance under linear scalings of the gray levels. Let $\tilde{\kappa}_f(p)$ denote the weak curvature of a function f at p . The following simple property will be used later.

PROPOSITION 4.3. *Let $u \in BV(\Omega)$ and $v = a + bu$ for some constants a and $b \neq 0$. Then for any $p \in \Omega$, $\tilde{\kappa}_u(p) = \tilde{\kappa}_v(p)$.*

With the help of the concept of weak curvature, the functionalized elastica energy (4.5) can be rigorously defined. A BV function u is said to be *admissible* if

$$\tilde{\kappa} \in L_2(D, d_u \nu).$$

For all such functions, the generalized elastica energy

$$J_2[u] = \int_D (a + b\tilde{\kappa}^2) d_u \nu \tag{4.9}$$

is well-defined and finite. Together with the boundary conditions (4.6), it defines the so called *elastica inpainting model*.

The elastica inpainting model is difficult for the existence and uniqueness analysis, due to the non-convexity of the energy and the involvement of curvature. However, there is indeed a special, simple, yet very useful case when one can carry out the analysis successfully. This is the TV inpainting model studied earlier by Chan and Shen [7].

4.3. The TV inpainting model of Chan and Shen. The TV inpainting model of Chan and Shen [7] is an extreme case of the elastica inpainting when one weighs highly against the total variation, i.e. $a/b = \infty$. Thus one is led to the minimization of

$$\text{TV}(u) = \int_{\Omega} |\nabla u|. \quad (4.10)$$

As in the study of minimal surfaces (De Giorgi [11]), the suitable companion condition becomes:

$$u|_{\Omega \setminus D} = u_0|_{\Omega \setminus D}, \quad (4.11)$$

where Ω is the entire (often rectangular) image domain. We shall always assume that Ω is a bounded Lipschitz domain. As in the study of minimal surfaces, Ω can be replaced by any open neighborhood of \bar{D} [7]. We call the combination the *noise free TV inpainting model*.

In [7] Chan and Shen focus on the general formulation, perceptual implications, computations, and various applications of the inpainting problem, as deeply inspired by the excellent work of Bertalmio et al. [2]. Here we present the existence theorem and discuss the uniqueness issue.

THEOREM 4.4 (Existence of a Noise Free TV Inpainting). *Suppose that the original complete image u_0 lies in $BV(\Omega)$, and takes gray values between 0 (black) and 1 (white). Then the noise free TV inpainting model (4.10) and (4.11), together with the gray value constraint $u \in [0, 1]$, has at least one optimal inpainting.*

Proof. Since the original complete image u_0 is admissible (i.e. satisfying the constraint and with finite TV measure), we can always find a minimizing sequence of admissible inpaintings $(u_n)_n$ for the model. Then both

$$\int_{\Omega} |\nabla u_n| \quad \text{and} \quad \int_{\Omega} |u_n(x)| dx$$

are bounded for all n since Ω is bounded and u_n takes values in the gray scale interval $[0, 1]$. By the weak compactness property of BV functions, there is a subsequence, still denoted by $(u_n)_n$ for convenience, which strongly converges to some $u_{\text{tv}} \in L_1(\Omega)$ in the L_1 norm. Apparently u_{tv} still meets the constraints

$$u_{\text{tv}}|_{\Omega \setminus D} = u_0|_{\Omega \setminus D} \quad \text{and} \quad u_{\text{tv}}(x) \in [0, 1].$$

Also by the L^1 lower semi-continuity property,

$$\int_{\Omega} |\nabla u_{\text{tv}}| \leq \liminf \int_{\Omega} |\nabla u_n| = \min_u \int_{\Omega} |\nabla u|.$$

Thus u_{tv} must be a minimizer. \square

Suppose in an application, we have *a priori* knowledge from the original complete image u_0 that there is a small open neighborhood O of ∂D , such that

$$\int_O |\nabla u_0| \leq \epsilon,$$

for some small constant ϵ . It means that the original image has very little jump along the inpainting domain (as controlled by ϵ). Then besides the constraint (4.11), we may also impose the boundary continuity condition

$$\int_O |\nabla u| \leq \epsilon. \quad (4.12)$$

Exactly in the same fashion of the proof, we can establish the existence theorem for this case.

Another important issue of inpainting is how to deal with noise, since in applications (such as the restoration of degraded photos or films), the left part of the image $u_0|_{\Omega \setminus D}$ is often noisy or containing misleading outliers (especially along the damaged boundary of D). Chan and Shen [7] modified the TV inpainting model for noisy images, in which the constraint (4.11) is replaced by the denoising one:

$$\frac{1}{\text{Area}(\Omega \setminus D)} \int_{\Omega \setminus D} (u - u_0)^2 = \sigma^2, \quad (4.13)$$

where σ^2 is the variation of the noise, which can be estimated from $u_0|_{\Omega \setminus D}$ by statistical estimators. By such constraint, we are assuming that hidden in u_0 is a “clean” image u_c such that

$$u_0(x) = u_c(x) + n(x),$$

where $n(x)$ is the noise independent of u_c . Since we only pay attention to its second order statistics, implicitly we are assuming that $n(x)$ is Gaussian with mean 0. Such setting appeared earlier in the classical TV denoising and deblurring model [28].

THEOREM 4.5 (Existence of a TV Inpainting for a Noisy Image). *Given an image observation u_0 on $\Omega \setminus D$, assume that there exists at least one image u_c (i.e. the original “clean” image) on Ω , which belongs to $BV(\Omega)$ and meets the denoising constraint (4.13) and gray scale constraint $u_c \in [0, 1]$. Then there exists at least one optimal TV inpainting on Ω , which does inpainting inside and noise cleaning outside.*

Proof. From the assumption on u_c , there exists a minimizing sequence of admissible inpaintings $(u_n)_n$. Thanks to the gray scale constraint, $(u_n)_n$ must be bounded in $BV(\Omega)$. Thus there is subsequence, still denoted by $(u_n)_n$ for convenience, which converges in L_1 norm to some $u_{\text{tv}} \in L_1(\Omega)$. Then the L_1 lower semi-continuity guarantees:

$$\int_{\Omega} |\nabla u_{\text{tv}}| \leq \liminf \int_{\Omega} |\nabla u_n| = \min_u \int_{\Omega} |\nabla u|.$$

We can further refine the subsequence so that

$$u_n \rightarrow u_{\text{tv}}, \quad \text{a.e. on } \Omega.$$

Thus u_{tv} must meet the gray scale constraint, and more importantly, by the Lebesgue Dominated Convergence Theorem,

$$\int_{\Omega \setminus D} (u_{\text{tv}} - u_0)^2 dx = \lim_n \int_{\Omega \setminus D} (u_n - u_0)^2 dx.$$

Therefore, u_{tv} is indeed an optimal TV inpainting. \square

REMARK 2. *If we drop the assumption that $u_0 \in [0, 1]$, and thus remove the gray scale constraint on u , then under the natural assumption (see [4]) that*

$$\sigma^2 \leq \frac{1}{\text{area}(\Omega \setminus D)} \int_{\Omega \setminus D} (u_0 - \langle u_0 \rangle)^2 dx < \infty,$$

one can still establish the existence theorem by applying Friedrich’s trace inequality [18] and Fatou’s lemma. (Here $\langle u_0 \rangle$ is the mean value of u_0 over the integration domain.)

The solutions to both TV and elastica inpaintings can be non-unique. But the models cannot carry all the blames for such non-uniqueness. In fact, the non-uniqueness can be eventually traced back to the inpainting problem itself.

To clarify the point, watch the image in Figure 4.1, whose middle square patch has been encrypted by a random image. We now try to inpaint the square to restore the original complete image.

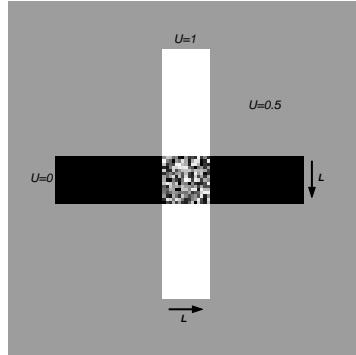


FIG. 4.1. *Non-uniqueness: who is to blame, the model or the problem itself?*

It seems that we have a black ($u = 0$) bar and white ($u = 1$) bar against a gray background ($u = 1/2$). A perceptually meaningful inpainting is to fill in either the black color so that the image shows a black bar occludes a farther white bar, or the white color for the opposite occlusion. Which one is more likely? The available part of the image (both the geometry and colors) is perfectly symmetric in terms of the two bars. Thus it is a half-half situation to human perception. Such perceptual uncertainty is the foundation for the non-uniqueness of inpainting models. In this sense, the non-uniqueness of an inpainting model (either the TV or elastica inpainting) is not to be blamed, but must be appreciated, since it potentially *models* the uncertainty of human perception in certain situations. (In terms of the Bayesian Decision Theory in vision analysis, this is the situation when the risk (or cost) is a competitive multimodal function.)

In many real applications, as Chan and Shen demonstrated in [6, 7], the solutions offered by the inpainting models seem always to be meaningful to human vision. This is because in applications, the locations and shapes of inpainting domains are randomly distributed.

4.4. Local analysis near a generic stationary point: $p < 3$. Generally, for any $p > 1$, one could also consider the p -elastica energy

$$J_p[u] = \int_{\Omega} (a + b|\kappa|^p) d_u \nu,$$

where $d_u \nu$ denoting the total variation measure of u , and if necessary, $|\kappa|$ is replaced by the weak absolute curvature $\tilde{\kappa}$. ($p = 1$ is less ideal since the *total curvature* energy allows sudden turns.) This general form of elasticity energy was also mentioned in Masnou and Morel [19]. So the question arises naturally: is there any essential difference between all different choices of p 's? We claim that indeed in some sense $p = 3$ is the threshold.

THEOREM 4.6. *Suppose u is C^2 near pixel z , and z is a generic stationary point of u in the sense that*

$$\nabla u(z) = 0 \quad \text{and} \quad H_u(z) \text{ is non-singular,}$$

where H_u is the 2 by 2 Hessian matrix of u . Then for all $p \geq 3$, $J_p[u] = \infty$.

In other words, generic stationary points are forbidden by the p -elasticity energy when $p \geq 3$. Apparently such restriction is not natural for image functions, and it thus seems that $p \in (1, 3)$ is a good choice, which of course includes Euler's energy $J_2[u]$.

Proof. Without loss of generality, assume that $z = (0, 0)$ and $u(z) = 0$. Since curvature is a second order feature, we can assume that u coincides with its second order Taylor expansion at z :

$$u(x) = u(x_1, x_2) = (x_1, x_2)A(x_1, x_2)^T,$$

where A is the non-singular Hessian $H_u(z)$. Thus A must be either elliptic or hyperbolic. Take the elliptic case for example. Since both $|\nabla u|$ and κ are invariant under Euclidean transforms, we can assume that

$$A = \text{diag}(\sigma_1^2, \sigma_2^2),$$

with $\sigma_1 \geq \sigma_2 > 0$. First we consider the case that $\sigma_1 = \sigma_2$. For convenience, we can assume that $\sigma_1 = 1$. Then $u = r^2 = x_1^2 + x_2^2$ and by Section 4.1

$$\begin{aligned} \int_{B_1} \kappa^p |\nabla u| dx &= \int_0^1 d\lambda \left(\int_{u=\lambda} \kappa^p ds \right) \\ &= \int_0^1 2r dr (2\pi r (1/r)^p) \\ &= 4\pi \int_0^1 (1/r)^{p-2} dr. \end{aligned}$$

Here for convenience, we have assumed that the C^2 neighborhood includes B_1 . Thus J_p on B_1 is finite if and only if $p < 3$, and as a result, when $p \geq 3$, J_p on Ω must blow up. The general case then follows easily by noticing that along any isophote (an ellipse):

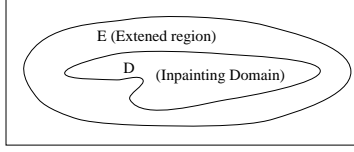
$$\sigma_1^2 x_1^2 + \sigma_2^2 x_2^2 = \lambda = r^2,$$

the curvature is bounded by

$$\frac{\sigma_1}{r} \geq \kappa \geq \frac{\sigma_2}{r}.$$

This completes the proof. \square

4.5. Relaxation of the constraints. The formulation of the elastica inpainting model (4.5) and (4.6) has been very much based on the image processing point of view as we have explained in the paragraphs that immediately follow it. But it is unclear whether the formulation is mathematically feasible. In fact, as well practiced in the theory of BV functions and minimal surfaces, it is often more manageable to formulate the problem on a larger domain than the original one. In this way, the boundary

FIG. 4.2. *Inpainting Domain D*

conditions are altered and naturally built into the energy functional itself. The TV inpainting model of Chan and Shen [7] mentioned above imparts this viewpoint. The same thing can be done for the general elastica inpaintings.

Let \$E\$ be a subset contained in \$\Omega \setminus D\$ such that \$E \cup D\$ is open and contains the closure of \$D\$ (see Figure (4.2)). For example, depending on the situation, we can simply take \$E = \Omega \setminus D\$. Suppose for the original image \$u_0\$,

$$J_2[u_0] = \int_{E \cup D} (a + b\tilde{\kappa}^2) d_{u_0} \nu$$

is finite. We inpaint \$u_0|_D\$ by the minimizer of

$$J_2[u] = \int_{E \cup D} (a + b\tilde{\kappa}^2) d_u \nu, \quad (4.14)$$

with the condition that

$$u|_E = u_0|_E. \quad (4.15)$$

In this way, the original other two regularity conditions across the boundary are approximately built into the energy itself, and need no extra care.

If the available part of the image in the vicinity of \$D\$ is corrupted by a homogeneous noise with variance \$\sigma^2\$, then the condition (4.15) is replaced by the fitting constraint:

$$\int_E |u - u_0|^2 dx = \sigma^2 \text{area}(E). \quad (4.16)$$

PROPOSITION 4.7. *Let \$u \in BV(E \cup D)\$ be a minimizer to the elastica inpainting (4.14) and (4.16). Then \$u\$ automatically satisfies the mean value constraint:*

$$\langle u \rangle = \langle u_0 \rangle,$$

where \$\langle f \rangle\$ denotes the mean value of \$f\$ over \$E\$.

Proof. The technique is similar to that used by Chambolle and Lions [4]. Assume otherwise the opposite situation occurs: \$\langle u \rangle \neq \langle u_0 \rangle\$. Define \$v = u - \langle u - u_0 \rangle\$. Then

$$\int_E |v - u_0|^2 dx = \int_E |u - u_0 - \langle u - u_0 \rangle|^2 dx < \int_E |u - u_0|^2 dx = \sigma^2 \text{area}(E).$$

where the strict inequality is due to the fact that among all constants, the mean is the only best \$L_2\$ fitting to a given signal. On the other hand, by the natural assumption of \$u_0\$ on \$E\$ in Remark 2,

$$\int_E |\langle v \rangle - u_0|^2 dx = \int_E |\langle u_0 \rangle - u_0|^2 dx \geq \sigma^2 \text{area}(E).$$

Therefore, there must exist some $s \in [0, 1]$ such that

$$\int_E |sv + (1-s)\langle v \rangle - u_0|^2 dx = \sigma^2 \text{ area}(E).$$

Define $w = sv + (1-s)\langle v \rangle$. By the invariant property of the weak curvature in Proposition 4.3, we have

$$J_2[w] = \int_{E \cup D} (a + b\tilde{\kappa}^2) |\nabla w| = s \int_{E \cup D} (a + b\tilde{\kappa}^2) |\nabla u| < \int_{E \cup D} (a + b\tilde{\kappa}^2) |\nabla u| = J_2[u],$$

where the strict inequality is due to the fact that u cannot be a constant, otherwise the constant must be $\langle u_0 \rangle$ because of the fitting constraint, which is impossible since the whole argument starts with $\langle u \rangle \neq \langle u_0 \rangle$. This eventually contradicts to the fact that u is a minimizer. \square

Finally, even the fitting constraint (4.16) can be built into the energy functional by minimizing

$$J_2^\lambda[u] = \int_{E \cup D} (a + b\tilde{\kappa}^2) |\nabla u| + \frac{\lambda}{2} \int_E (u - u_0)^2 dx. \quad (4.17)$$

It can also be easily shown that a minimizer of $J_2^\lambda[u]$ automatically satisfies the mean value constraint.

The last formulation bears a formal Bayesian explanation as Mumford did for various segmentation models [22]. From the probability point of view, formally, the conditional probability

$$P(u_0|u) = \text{const. exp} \left(-\lambda/2 \int_E (u - u_0)^2 dx \right)$$

is the *data model* or *generative model*, and probability

$$P(u) = \text{const. exp}(-J_2[u])$$

is the *prior model*. Together, the minimization of $J_2^\lambda[u]$ corresponds to the method of MAP, or *Maximum a Posteriori*. The data model hints that the best fitting constant λ should be proportional to $1/\sigma^2$, the reciprocal of the variance, which can be very helpful in numerical computations (Chan, Osher and Shen [5]). On the other hand, the prior model can be traced back to Mumford's Bayesian rationale for Euler's elastica being a prior curve model, as discussed in Section 2.

5. The Euler-Lagrange Equation. The direct method for the variational elastica inpainting is difficult due to the geometric quantity - curvature. Notice that the curvature has even no linear structure. That is, one cannot say much about the curvature κ_{u+v} of the summation even the precise information on κ_u and κ_v is available. Such obstacle blocks classical linear approaches based on Sobolev spaces or BV spaces.

In this situation, as well practiced in the PDE method in image processing, one is led to the study of the formal Euler-Lagrange equation. Often the PDE's can handle geometry better than the variational problem itself, as in the case of *mean curvature motions* [20].

In this section, we first derive the formal Euler-Lagrange equation for the fitted elastica inpainting model (4.17), and then interpret it geometrically. We will show that the geometric meaning unifies the early method of Bertalmio, et al. [2] based

on transportation PDEs and that of Chan and Shen [6] based on curvature driven diffusions, though the two have been obtained from very different considerations originally. We conjecture that transportation and CDD are the two universal mechanisms for any low-level non-texture inpainting.

5.1. The derivation of the Euler-Lagrange equation. In the formal derivation, we shall always assume that the image is smooth enough, say in $W^{2,1}$, and the curvature is well defined. The variation δu is always assumed to have compact support so that integration by parts can be carried out without the boundary term.

THEOREM 5.1. *Let $\phi \in C^1(R, [0, \infty))$ be a given function and*

$$R[u] = \int_{E \cup D} \phi(\kappa) |\nabla u| dx.$$

Then the first variation is given by

$$\frac{\partial R}{\partial u} = -\nabla \cdot \vec{V},$$

where the flux field \vec{V} is

$$\vec{V} = \phi(\kappa) \vec{n} - \frac{\vec{t}}{|\nabla u|} \frac{\partial (\phi'(\kappa) |\nabla u|)}{\partial \vec{t}}. \quad (5.1)$$

Here \vec{n} is the ascending normal field $\nabla u / |\nabla u|$, and \vec{t} is the tangent field (whose exact orientation does not matter due to the parity of \vec{t} in the expression). (See Figure 5.1.)

Proof. For much of the convenience to come, write $\langle f \rangle = \int_{E \cup D} f dx$. Then,

$$\begin{aligned} \delta R &= \langle \delta(|\nabla u| \phi(\kappa)) \rangle \\ &= \langle \phi(\kappa) \delta |\nabla u| \rangle + \langle |\nabla u| \delta \phi(\kappa) \rangle \\ &= \langle \phi(\kappa) \frac{\nabla u}{|\nabla u|} \delta \nabla u \rangle + \langle \phi'(\kappa) |\nabla u| \delta \kappa \rangle \\ &= -\langle \nabla \cdot [\phi(\kappa) \vec{n}] \delta u \rangle + \langle \phi'(\kappa) |\nabla u| \delta \kappa \rangle. \end{aligned}$$

Thus we need work out the variation of curvature:

$$\begin{aligned} \delta \kappa &= \delta(\nabla \cdot \frac{\nabla u}{|\nabla u|}) = \nabla \cdot [\frac{1}{|\nabla u|} \nabla(\delta u) + \nabla u \delta(\frac{1}{|\nabla u|})] \\ &= \nabla \cdot [\frac{1}{|\nabla u|} \nabla(\delta u) - (\nabla u \frac{\nabla u}{|\nabla u|^3}) \nabla(\delta u)] \\ &= \nabla \cdot [\frac{1}{|\nabla u|} \{I - \vec{n} \otimes \vec{n}\} \nabla(\delta u)]. \end{aligned}$$

Here I denote the identity transform, and $P = \vec{n} \otimes \vec{n}$ is the orthogonal projection onto the normal direction. Therefore

$$\begin{aligned} \langle \phi'(\kappa) |\nabla u| \delta \kappa \rangle &= \langle \phi'(\kappa) |\nabla u| \nabla \cdot [\frac{1}{|\nabla u|} \{I - \vec{n} \otimes \vec{n}\} \nabla(\delta u)] \rangle \\ &= \langle -\nabla(\phi'(\kappa) |\nabla u|) [\frac{1}{|\nabla u|} \{I - \vec{n} \otimes \vec{n}\} \nabla(\delta u)] \rangle \\ &= \langle -\{I - \vec{n} \otimes \vec{n}\} \{\frac{1}{|\nabla u|} \nabla(\phi'(\kappa) |\nabla u|)\} \nabla(\delta u) \rangle \\ &= \langle \nabla \cdot [(I - \vec{n} \otimes \vec{n}) \{\frac{1}{|\nabla u|} \nabla(\phi'(\kappa) |\nabla u|)\}] \delta u \rangle, \end{aligned}$$

where we have applied the fact that $I - P$ is symmetric. Therefore

$$\begin{aligned}\frac{\partial R}{\partial u} &= -\nabla \cdot [\phi(\kappa)\vec{n} - \frac{1}{|\nabla u|}(I - \vec{n} \otimes \vec{n})\nabla(\phi'(\kappa)|\nabla u|)] \\ &= -\nabla \cdot [\phi(\kappa)\vec{n} - \frac{1}{|\nabla u|} \frac{\partial(\phi'(\kappa)|\nabla u|)}{\partial \vec{t}} \vec{t}] \\ &= -\nabla \cdot \vec{V}.\end{aligned}$$

We have used the fact that $I = \vec{n} \otimes \vec{n} + \vec{t} \otimes \vec{t}$, and $\vec{t} \otimes \vec{t} \nabla f = \vec{t} \partial f / \partial \vec{t}$. This completes the proof.

□

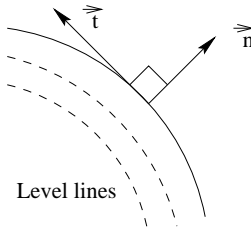


FIG. 5.1. The normal and tangent vectors.

Thus the gradient of a general functional $R[u]$ is in the divergence form. The vector field \vec{V} shall be called the *flux field* of $R[u]$. The theorem shows that the flux field has a natural decomposition in the normal and tangent fields. Moreover, it is *morphologically invariant*.

PROPOSITION 5.2. *The flux field \vec{V} is morphologically invariant.*

Proof. Let g be any (smooth) morphological transform of the gray scales:

$$u \rightarrow g(u), \quad g'(u) > 0.$$

we need show that for any image u , the fluxes $\vec{V}_u = \vec{V}_{g(u)}$. Notice that κ , \vec{n} , and \vec{t} are all morphologically invariant. Moreover,

$$\begin{aligned}\frac{1}{|\nabla g(u)|} \frac{\partial(\phi'(\kappa)|\nabla g(u)|)}{\partial \vec{t}} \vec{t} &= \frac{1}{g'(u)|\nabla u|} \frac{\partial(g'(u)\phi'(\kappa)|\nabla u|)}{\partial \vec{t}} \vec{t} \\ &= \frac{g'(u)}{g'(u)|\nabla u|} \frac{\partial(\phi'(\kappa)|\nabla u|)}{\partial \vec{t}} \vec{t} = \frac{1}{|\nabla u|} \frac{\partial(\phi'(\kappa)|\nabla u|)}{\partial \vec{t}} \vec{t},\end{aligned}$$

where we have applied the fact that u , and therefore $g'(u)$ are both constants in the tangent direction. Thus $\vec{V}_{g(u)} = \vec{V}_u$. □

Masnou and Morel (private communication) also worked out the Euler-Lagrange equation (5.1) earlier, though it was not expressed in the above concise geometric formula.

COROLLARY 5.3. *For the elastica inpainting model (4.17), the gradient is*

$$\frac{\partial J_2^\lambda[u]}{\partial u} = -\nabla \cdot \vec{V} + \lambda_E (u - u_0),$$

where,

$$\vec{V} = (a + b\kappa^2) \vec{n} - \frac{2b}{|\nabla u|} \frac{\partial \kappa |\nabla u|}{\partial t} \vec{t}, \quad (5.2)$$

$$\lambda_E(x) = \lambda \cdot \mathbf{1}_E(x), \quad \text{the indicator of } E. \quad (5.3)$$

Therefore, the infinitesimal steepest descent marching is

$$\frac{\partial u}{\partial t} = \nabla \cdot \vec{V} - \lambda_E(u - u_0). \quad (5.4)$$

In numerical computation, as Marquina and Osher [17] proposed, the weighted steepest descent method generally converges faster than the original one:

$$\frac{\partial u}{\partial t} = |\nabla u| \nabla \cdot \vec{V} - |\nabla u| \lambda_E(u - u_0). \quad (5.5)$$

By such modification, without the fitting term, the evolution equation is morphologically invariant since the flux field is and the $g'(u)$ factors cancel out each other from $\partial u / \partial t$ and $|\nabla u|$. If further $b = 0$, we have the well known *mean curvature motion* [20].

Our numerical PDE scheme in the coming section is applied to the modified steepest descent equation (5.5).

5.2. The inpainting mechanisms of transportation and diffusion. We now show that the flux field \vec{V} beautifully offers a unified viewpoint on the earlier work of Bertalmio et al. on *transportation* based inpainting [2] and that of Chan and Shen [7] on CDD (curvature driven diffusions) based inpainting. In return, these earlier works reveal the fine structure of elastica inpaintings from the PDE point of view.

The first PDE based inpainting model of Bertalmio et al. [2] is based on the beautiful intuition of smoothness transportation along isophotes:

$$\frac{\partial u}{\partial t} = \nabla^\perp u \cdot \nabla L(u), \quad (5.6)$$

where, $\nabla^\perp u = (-u_y, u_x) = |\nabla u| \vec{t}$ is the 90-degree-rotated normal vector, and $L(u)$ can be any smoothness measure of the image u . For example, in the numerical experiment of [2], L is chosen to be the Laplacian Δu . The model carries the transportation nature since as the evolution approaches its equilibrium state, we have

$$\vec{t} \cdot \nabla L(u) = 0 \quad \text{and} \quad \frac{\partial L(u)}{\partial t} = 0,$$

which means, along an isophote, the smoothness measure is conserved. Thus in terms of the available boundary data, the image evolves like transporting the boundary smoothness along the extended isophotes into the inpainting domain.

However, due to the lack of communications among the isophotes, the transportation may result in kinks or contradictions inside the inpainting domain, just as shocks may develop in traffic models. Thus in [2], the equation (5.6) is implemented with the help of intermediate steps of anisotropic diffusions. As we shall see below, such intuition is well backed up by the elastica inpainting.

On the other hand, in [6], in order to realize the so-called *Connectivity Principle* in perceptual disocclusion, Chan and Shen proposed the CDD inpainting model:

$$\frac{\partial u}{\partial t} = \nabla \cdot \left(\frac{g(\kappa)}{|\nabla u|} \nabla u \right), \quad (5.7)$$

where $g : R \rightarrow [0, +\infty)$ is a continuous function satisfying $g(0) = 0$ and $g(\pm\infty) = +\infty$. If the position of g is replaced by 1, then this is the classical TV anisotropic diffusion. The introduction of $g(\kappa)$ is to penalize large curvatures and encourage small ones, since $D = g(\kappa)/|\nabla u|$ is physically the diffusivity coefficient. Under such action, objects (like a black bar) broken by the inpainting domains are generally encouraged to be reconnected, since separated parts usually have curved or cornered fronts with large curvatures.

It has remained a mystery why we can have two seemingly very different inpainting mechanisms: the model in [2] transports information *along* isophotes, while the CDD (and TV) inpainting model [6] diffuses information *across*. We now explain that the elastica inpainting model unifies the two by bearing both the transportation and CDD mechanisms.

We have established in Theorem 5.1 that the flux \vec{V} for the inpainting energy $R[u]$ consists of two components: the normal part

$$\vec{V}_n = \phi(\kappa) \vec{n},$$

and the tangential part

$$\vec{V}_t = -\frac{1}{|\nabla u|} \frac{\partial(\phi'(\kappa)|\nabla u|)}{\partial \vec{t}} \vec{t}.$$

Therefore, the normal flux \vec{V}_n exactly corresponds to Chan and Shen's CDD program (5.7) with

$$g(\kappa) = \phi(\kappa).$$

The different requirements on g and ϕ is due to the fact that the CDD inpainting scheme is based on the diffusion only. On the other hand, the tangential component can be written as

$$\vec{V}_t = -\left(\frac{1}{|\nabla u|^2} \frac{\partial(\phi'(\kappa)|\nabla u|)}{\partial \vec{t}} \right) \nabla^\perp u,$$

and thus its divergence

$$\nabla \cdot \vec{V}_t = \nabla^\perp u \cdot \nabla \left(\frac{-1}{|\nabla u|^2} \frac{\partial(\phi'(\kappa)|\nabla u|)}{\partial \vec{t}} \right),$$

since $\nabla^\perp u$ is divergence free, which corresponds exactly to Bertalmio et al.'s scheme (5.6) with the smoothness measure given by

$$L_\phi = \frac{-1}{|\nabla u|^2} \frac{\partial(\phi'(\kappa)|\nabla u|)}{\partial \vec{t}}.$$

We can further work out the expression to

$$L_\phi = \frac{-1}{|\nabla u|^2} \left(|\nabla u| \phi''(\kappa) \frac{\partial \kappa}{\partial \vec{t}} + \phi'(\kappa) [\nabla \otimes \nabla u](\vec{n}, \vec{t}) \right).$$

Here $[\nabla \otimes \nabla u](\bullet, \bullet)$ is the Hessian bilinear form of u . Thus in a simple case like $\phi(s) = |s|$, and $\kappa \neq 0$, we have

$$L_\phi = \frac{\pm 1}{|\nabla u|^2} [\nabla \otimes \nabla u](\vec{n}, \vec{t}),$$

which, up to a multiplicative rescaling, resembles the choice of Laplacian in [2]:

$$\Delta u = \text{trace}(\nabla \otimes \nabla u) = [\nabla \otimes \nabla u](\vec{n}, \vec{n}) + [\nabla \otimes \nabla u](\vec{t}, \vec{t}).$$

In summary, the elastica inpainting scheme combines both the transportation mechanism of Bertalmio et al.'s model and the CDD mechanism of Chan and Shen's model. It thus provides a theoretical foundation for these two earlier works on PDE based image inpaintings. In return, the earlier works also shed lights on the meaning of the flux field \vec{V} and the interpretation of the elastica or curvature based variational inpaintings. In particular, we are assured by the existing works that the numerical PDE approach will be feasible, although the direct variational method has turned out to be very difficult.

6. Computation and Examples.

6.1. Numerical implementation. In this section, we explain the numerical scheme for the evolution equation (5.5):

$$\frac{\partial u}{\partial t} = |\nabla u| \nabla \cdot \vec{V} - |\nabla u| \lambda_E (u - u_0),$$

where the flux \vec{V} and λ_E are as given in Corollary 5.3. Remind our readers that the factor $|\nabla u|$, as suggested by Marquina and Osher in [17], is for accelerating the time marching. (In computation, the factor may be replaced by its regularized one $|\nabla u|_\epsilon = \sqrt{\epsilon^2 + |\nabla u|^2}$.)

Let (i, j) denote the digital pixel locations, and time be digitized to $n = 0, 1, \dots$ with a chosen small time step h . Thus $u_{(i,j)}^n$ denotes the value of u at pixel (i, j) at time nh . Then

$$u_{(i,j)}^{n+1} = u_{(i,j)}^n + h \left(|\nabla u_{(i,j)}^n| F(u_{(i,j)}^n) - |\nabla u_{(i,j)}^n| \lambda_{E,(i,j)} (u_{(i,j)}^n - u_{0,(i,j)}) \right),$$

where $F(u_{(i,j)}^n) = \nabla \cdot \vec{V}_{(i,j)}^n$ and u_0 is the available image.

We now focus on the spatial digitization of the right hand side at a fixed time nh . Thus we shall conveniently leave out the superscript n . Following Marquina and Osher [17], the accelerating factor $|\nabla u_{(i,j)}|$ in front of $F(u_{(i,j)})$ is approximated by the central differencing:

$$|\nabla u_{(i,j)}| = \frac{1}{2} \sqrt{(u_{(i+1,j)} - u_{(i-1,j)})^2 + (u_{(i,j+1)} - u_{(i,j-1)})^2}, \quad (6.1)$$

and the factor $|\nabla u_{(i,j)}|$ in front of $\lambda_{E,(i,j)} (u_{(i,j)} - u_{0,(i,j)})$ by the upwind scheme:

$$|\nabla u_{(i,j)}| = \sqrt{(\text{upwind } D_x u_{(i,j)})^2 + (\text{upwind } D_y u_{(i,j)})^2}$$

$$\text{upwind } D_x u_{(i,j)} = \begin{cases} \frac{1}{2}(u_{(i,j)} - u_{(i-1,j)}) & \text{if } (u_{(i+1,j)} - u_{(i-1,j)})(u_{(i,j)} - u_{0,(i,j)}) > 0 \\ \frac{1}{2}(u_{(i+1,j)} - u_{(i,j)}) & \text{if } (u_{(i+1,j)} - u_{(i-1,j)})(u_{(i,j)} - u_{0,(i,j)}) < 0 \end{cases} \blacksquare$$

The upwinding on y is similar.

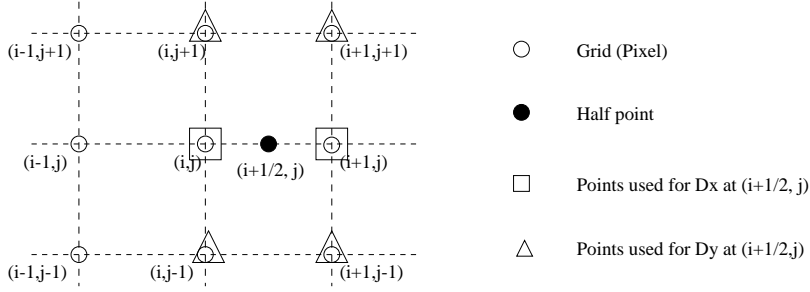


FIG. 6.1. Grid for the finite differencings

Now we focus on the discretization of $F(u_{(i,j)}) = \nabla \cdot \vec{V}_{(i,j)}$. Write $\vec{V} = (V^1, V^2)$, and

$$\vec{n} = (n^1, n^2) = \left(\frac{u_x}{|\nabla u|}, \frac{u_y}{|\nabla u|} \right), \quad \vec{t} = (t^1, t^2) = \left(-\frac{u_y}{|\nabla u|}, \frac{u_x}{|\nabla u|} \right).$$

Then

$$\begin{aligned} V^1 &= (a + b\kappa^2) n^1 - \frac{2b}{|\nabla u|} (t^1 D_x(\kappa |\nabla u|) + t^2 D_y(\kappa |\nabla u|)) t^1 \\ &= (a + b\kappa^2) \frac{D_x u}{|\nabla u|} + \frac{2b}{|\nabla u|^3} (-D_y u D_x(\kappa |\nabla u|) + D_x u D_y(\kappa |\nabla u|)) D_y u, \end{aligned}$$

where the partial derivative symbols D_x and D_y are introduced to ease the placement of subscripts. The expression of V^2 can be worked out similarly. Based on the half-point central differencing, we have

$$\begin{aligned} F(u_{(i,j)}) &= \nabla \cdot \vec{V}_{(i,j)} = D_x V_{(i,j)}^1 + D_y V_{(i,j)}^2 \\ &= \left(V_{(i+\frac{1}{2},j)}^1 - V_{(i-\frac{1}{2},j)}^1 \right) + \left(V_{(i,j+\frac{1}{2})}^2 - V_{(i,j-\frac{1}{2})}^2 \right). \end{aligned}$$

Thus we need specify the *half-point* values for all the involved quantities. Take the x -half-point $(i+1/2, j)$ for example. For the curvature, we take the min-mod [25] between the *whole* pixels:

$$\kappa_{(i+\frac{1}{2},j)} = \text{minmod}(\kappa_{(i+1,j)}, \kappa_{(i,j)}), \quad \text{minmod}(\alpha, \beta) = \frac{\text{sign}(\alpha) + \text{sign}(\beta)}{2} \min(|\alpha|, |\beta|).$$

D_x 's at an x -half-point $(i+1/2, j)$ are approximated by the central differencing of the two adjacent whole pixels $(i+1, j)$ and (i, j) . For examples (see Figure 6.1),

$$\begin{aligned} D_x u_{(i+1/2,j)} &= \frac{1}{2} (u_{(i+1,j)} - u_{(i,j)}) \\ D_x(\kappa |\nabla u|)_{(i+1/2,j)} &= \frac{1}{2} (\kappa_{(i+1,j)} |\nabla u|_{(i+1,j)} - \kappa_{(i,j)} |\nabla u|_{(i,j)}). \end{aligned}$$

Here $|\nabla u|_{(i,j)}$ is as in (6.1). D_y 's at an x -half-point $(i+1/2, j)$ are approximated by the min-mod of D_y 's at the two adjacent whole pixels $(i+1, j)$ and (i, j) (see Figure 6.1). For instance, for $D_y u_{(i+1/2,j)}$,

$$D_y u_{(i+1/2,j)} = \text{minmod} \left(\frac{1}{2} (u_{(i+1,j+1)} - u_{(i+1,j-1)}), \frac{1}{2} (u_{(i,j+1)} - u_{(i,j-1)}) \right). \quad (6.2)$$

The same thing can be done for $D_y(\kappa|\nabla u|)$ at $(i + 1/2, j)$. Then $|\nabla u|^2$ at $(i + 1/2, j)$ is naturally defined as the sum of squares of $D_x u_{(i+1/2,j)}$ and $D_y u_{(i+1/2,j)}$. Therefore, eventually, all quantities involved are expressed by the gray levels $u_{(i,j)}$ at all whole pixels.

Numerical experiments in Figure 6.2 have shown the advantage of the min-mod discretization for D_y at x -half-points, compared with other two competing methods ($w = u$ or $\kappa|\nabla u|$): the *forward* substitution of $D_y w_{(i+1/2,j)}$ by $D_y w_{(i,j)}$, and the *average* substitution by

$$\frac{1}{4} (u_{(i+1,j+1)} - u_{(i+1,j-1)} + u_{(i,j+1)} - u_{(i,j-1)}) .$$

As in computational fluid dynamics, the min-mod method seems to catch sharper edges (or *shocks*) and result in less blurring.

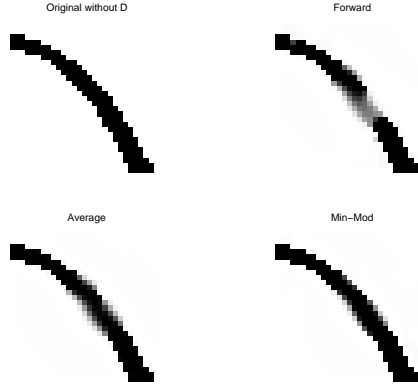


FIG. 6.2. Experimental results show the advantage of the min-mod discretization in (6.2). The upper left one is the original complete image of a ribbon. The inpainting domain is a square covering the middle part of ribbon. The other three images are the outputs of the numerical inpainting schemes based on the forward substitution, the average discretization, and the min-mod discretization, separately. (See the section for more details.) The min-mod scheme seems to yield better edge sharpness, as expected from the shock wave computations in computational fluid dynamics.

6.2. Examples. In this section, we show several numerical examples of elastica inpaintings.

Figure 6.3 shows an application of the TV inpainting model (with $b = 0$ in the elastica model) in text removal. As we mentioned earlier, one major advantage of the numerical PDE approach over the dynamical programming algorithm is its permission of arbitrary topology of the inpainting domain. The letters in this example indeed demand such permission.

Figure 6.4 demonstrates a photo shop application of elastica inpaintings in the digital restoration of an old scratched photograph. (Image source: [2].) The example shows what an inpainting model must be able to accomplish: to consistently reconnect all the broken isophotes, including broken edges with low contrasts (like the shadow of the nose).

The next two figures explain two effects of curvature based inpaintings. The example in Figure 6.5 shows that if more weights are put against the curvature term in the elastica model, the inpainted isophotes and edges become smoother and perceptually better. The second example in Figure 6.6 explains that as more weights are put



FIG. 6.3. An example of TV inpainting for text removal, with $b = 0$ in the elastica model.

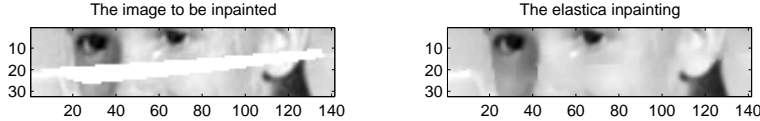


FIG. 6.4. An example of elastica inpainting for scratch removal in an old black-white photograph.

against the curvature term, the model tends to favor the *Connectivity Principle* in perception [6, 24]. That is, unlike the extreme case of the TV inpainting, the model encourages connection.

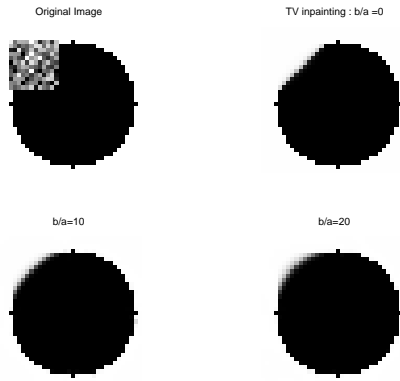


FIG. 6.5. Effect I of elastica inpaintings: a larger weight b against the curvature term produces smoother isophotes and edges, and better visual results.

The last figure shows two more examples of elastica inpaintings, where one can further appreciate the power of the elastica inpainting model and the numerical PDE approach. Large scale “communications” among the separated parts are made possible simply because of a good image or curve prior model — Euler’s elasticas.

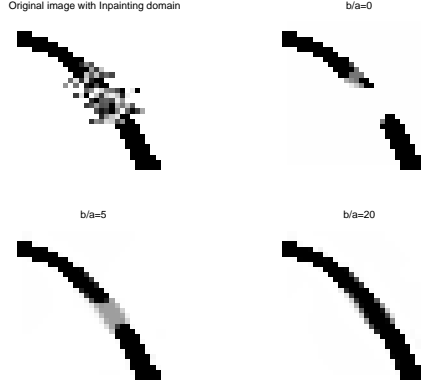


FIG. 6.6. *Effect II of elastica inpaintings: a large weight b against the curvature term favors the Connectivity Principle: the model encourages the connection of separated parts.*

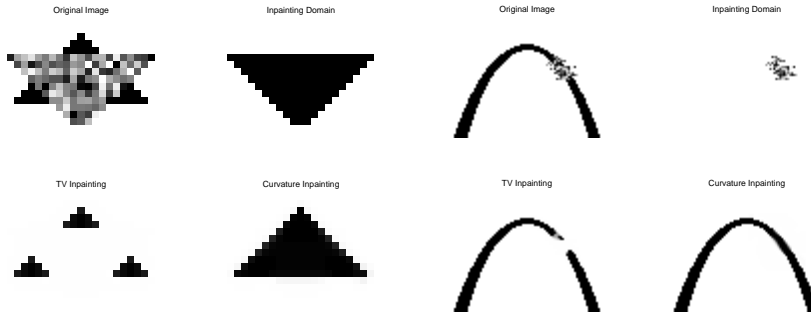


FIG. 6.7. *Two more examples of elastica inpaintings.*

Acknowledgments. The authors thank Professor Sapiro's group in ECE, University of Minnesota, for their generous teaching and help on the inpainting topic. We would also like to thank Professors Stanley Osher and Vese Luminita (UCLA), Li-Tien Cheng (UC San Diego), Simon Masnou and Jean-Michel Morel (France), Peter Olver, Robert Gulliver, Fadil Santosa, Dan Kersten, and Selim Esedoglu (University of Minnesota) for their suggestions and help.

REFERENCES

- [1] C. Ballester, M. Bertalmio, V. Caselles, G. Sapiro, and J. Verdera. Filling-in by joining interpolation of vector fields and grey levels. IMA Technical Report, *University of Minnesota*, may, 2000.
- [2] M. Bertalmio, G. Sapiro, V. Caselles, and C. Ballester. Image inpainting. Computer Graphics, *SIGGRAPH 2000*, July, 2000.
- [3] G. Birkhoff and C. R. De Boor. Piecewise polynomial interpolation and approximation. In H. Garabedian, editor, *Approximation of Functions*, pages 164–190. Elsevier, 1965.
- [4] A. Chambolle and P. L. Lions. Image recovery via Total Variational minimization and related problems. *Numer. Math.*, 76:167–188, 1997.
- [5] T. Chan, S. Osher, and J. Shen. The digital TV filter and nonlinear denoising. *IEEE Trans. Image Process.*, 10(2):231–241, 2001.
- [6] T. Chan and J. Shen. Non-texture inpainting by curvature driven diffusions (CDD). *J. Visual Comm. Image Rep.*, submitted, 2000.
- [7] T. Chan and J. Shen. Mathematical models for local non-texture inpaintings. *SIAM J. Appl. Math.*, to appear, 2001.

- [8] S. S. Chern, W. H. Chen, and K. S. Lam. *Lectures on Differential Geometry*. World Scientific, New Jersey, 1998.
- [9] G. Emile-Male. *The Restorer's Handbook of Easel Painting*. Van Nostrand Reinhold, New York, 1976.
- [10] S. Geman and D. Geman. Stochastic relaxation, Gibbs distributions, and the Bayesian restoration of images. *IEEE Trans. Pattern Anal. Machine Intell.*, 6:721–741, 1984.
- [11] E. De Giorgi. Frontiere orientate di misura minima. *Sem. Mat. Scuola Norm. Sup. Pisa*, 1960–61.
- [12] E. Giusti. *Minimal Surfaces and Functions of Bounded Variation*. Birkhäuser, Boston, 1984.
- [13] G. H. Golub and J. M. Ortega. *Scientific Computing and Differential Equations*. Academic Press, 1992.
- [14] D. C. Knill and W. Richards. *Perception as Bayesian Inference*. Cambridge Univ. Press, 1996.
- [15] J. Langer and D. A. Singer. The total squared curvature of closed curves. *J. Diff. Geom.*, 20:1–22, 1984.
- [16] A. E. H. Love. *A Treatise on the Mathematical Theory of Elasticity*. Dover, New York, 4th ed., 1927.
- [17] A. Marquina and S. Osher. *Lecture Notes in Computer Science*, volume 1682, chapter “A new time dependent model based on level set motion for nonlinear deblurring and noise removal”, pages 429–434. 1999.
- [18] J. T. Marti. *Introduction to Sobolev Spaces and Finite Element Solution of Elliptic Boundary Value Problems*. Academic Press, 1986.
- [19] S. Masnou and J.-M. Morel. Level-lines based disocclusion. *Proceedings of 5th IEEE Int'l Conf. on Image Process., Chicago*, 3:259–263, 1998.
- [20] J.-M. Morel and S. Solimini. *Variational Methods in Image Segmentation*, volume 14 of *Progress in Nonlinear Differential Equations and Their Applications*. Birkhäuser, Boston, 1995.
- [21] D. Mumford. Elastica and computer vision. In C. L. Bajaj, editor, *Algebraic Geometry and its Applications*, pages 491–506. Springer-Verlag, New York, 1994.
- [22] D. Mumford. *Geometry Driven Diffusion in Computer Vision*, chapter “The Bayesian rationale for energy functionals”, pages 141–153. Kluwer Academic, 1994.
- [23] D. Mumford and J. Shah. Optimal approximations by piecewise smooth functions and associated variational problems. *Comm. Pure Applied. Math.*, XLII:577–685, 1989.
- [24] M. Nitzberg, D. Mumford, and T. Shiota. *Filtering, Segmentation, and Depth*. Lecture Notes in Comp. Sci., Vol. 662. Springer-Verlag, Berlin, 1993.
- [25] S. Osher and L. Rudin. Feature-oriented image enhancement using shock filters. *SIAM J. Num. Anal.*, 27(4):919–940, 1990.
- [26] S. Osher and J. A. Sethian. Fronts propagating with curvature-dependent speed: Algorithms based on Hamilton-Jacobi formulations. *J. Comput. Phys.*, 79(12), 1988.
- [27] L. Rudin and S. Osher. Total variation based image restoration with free local constraints. *Proc. 1st IEEE ICIP*, 1:31–35, 1994.
- [28] L. Rudin, S. Osher, and E. Fatemi. Nonlinear total variation based noise removal algorithms. *Physica D*, 60:259–268, 1992.
- [29] G. Strang. *Introduction to Applied Mathematics*. Wellesley-Cambridge Press, MA, 1993.
- [30] S. Walden. *The Ravished Image*. St. Martin's Press, New York, 1985.